ARCHIVE OF MECHANICAL ENGINEERING

DOI: 10.24425/ame.2023.148698 2023, Vol. 70, No. 4, pp. 531–551

Bowen JIAO [1], Qiang BIAN [1], Xinghong WANG[1], Chunjiang ZHAO [1], Ming CHEN[1], Xiangyun ZHANG[2]

Analysis of high-speed angular ball bearing lubrication based on bi-directional fluid-solid coupling

Received 22 July 2023, **Revised** 13 November 2023, **Accepted** 16 November 2023, **Published online** 20 December 2023

Keywords: angular contact ball bearings, fluid-structure-interaction, bi-directional coupling, lubrication

The lubrication of angular contact ball bearings under high-speed motion conditions is particularly important to the working performance of rolling bearings. Combining the contact characteristics of fluid domain and solid domain, a lubrication calculation model for angular contact ball bearings is established based on the RNG k-ε method. The pressure and velocity characteristics of the bearing basin under the conditions of rotational speed, number of balls and lubricant parameters are analyzed, and the lubrication conditions and dynamics of the angular contact ball bearings under different working conditions are obtained. The results show that the lubricant film pressure will rise with increasing speed and viscosity of the lubricant. The number of balls affects the pressure and velocity distribution of the flow field inside the bearing but has a small effect on the values of the characteristic parameters of the bearing flow field. The established CFD model provides a new approach to study the effect of fluid flow on bearing performance in angular contact ball bearings.

1. Introduction

Angular contact ball bearings are a type of crucial mechanical support element that is used in high-speed machine machines, aerospace engines, and other precision equipment [1, 2]. One of the primary elements influencing the motion state of angular contact ball bearings are lubrication properties; inadequate lubrication

✉ Chunjiang ZHAO, e-mail: zhaochj75@163.com

[1]School of Mechanical Engineering, Taiyuan University of Science and Technology, Taiyuan, China. ORCIDs: B.J.: 0009-0000-3822-7823; Q.B.: 0009-0001-9500-421X; C.Z: 0000-0003-1327-3756

[2]Luoyang Bearing Research Institute Co., Ltd, Luoyang, China

will result in early bearing failure and financial losses [3–5]. In order to enhance bearing performance, it is crucial to research the lubricating properties of bearings.

With the development of elastic fluid theory, it was found that a flexible liquid oil film exists at the location where the ball contacts the inner and outer raceway inside the bearing. In order to accurately derive the thickness, shape and pressure distribution of the elastohydrodynamic oil film, Harris [6] developed a new analytical model for ball bearings based on the theory of elastic fluid lubrication. Wang et al. [7] established an elastohydrodynamic model to study the load variation rules, minimum oil film thickness, and maximum oil film pressure of the bearing. The results show that with the increase of system oil supply and lubricant viscosity, the temperature rise of the outer ring of the bearing increases firstly, then decreases, and finally increases again. Zhou et al. [8] present an equivalent integral form of the static Reynolds equation based on the finite element method and the variational principle. The effects of diameter, lubricant viscosity, and external load on the equilibrium position and internal pressure were further investigated.

Due to the continuous development of computer computing power, so that the original, almost unsolvable complex equations can be solved, more and more researchers and scholars choose to use the fluid-solid coupling method to solve the lubrication problem. Chmelař et al. [9] created a method for predicting the lubrication state of roller bearings using a single axial radial load as input. The lubrication state was evaluated, taking into account the surface roughness. The results showed that rotational speed and lubricant viscosity were the main factors influencing the thickness of the elastohydrodynamic lubrication film. Wang et al. [10] investigated the effect of oil supply on lubrication performance through a single coupled simulation and experiment. The results show that the bottom oil layer is the key to realizing the oil-boosting effect, and its distribution can reflect the effect of oil-boosting lubrication. Xie et al. [11] proposed a modified plain-bearing lubrication model considering the effects of various coupling factors. The gap ratio was found to have a significant effect on the static performance parameters and dynamic coefficients of the inner film. Almeida et al. [12] analyzed sliding friction on a microscopic scale using a three-dimensional model and developed a fluid-solid coupling model for the lubricated contact portion of a bearing surface. The effect of lubricant film thickness on friction under hydrodynamic and mixed lubrication conditions was investigated. The results show that the computational model can exhibit the effect of lubrication on the contact between rough surfaces.

At present, certain outcomes have been obtained in the study of bearing model calculation employing numerical computation techniques. However, the interaction properties between the fluid and solid domains must be taken into account when calculating the local lubrication contact of bearings, which significantly raises the model's complexity and calculation difficulties. Furthermore, there are few computations of the bidirectional interaction between the fluid and the solid, and the research models that are now in use only take into account the unidirectional interaction in the fluid domain. Therefore, the research on the bidirectional action

of rolling bearing transient lubrication must be further deepened and improved. In order to tackle this issue, a fluid lubrication calculation model for angular contact ball bearings is established based on the RNG k-ε method by combining the contact characteristics of fluid and solid domains. Angular contact ball bearings' dynamic contact and lubrication properties are investigated in relation to varying inner ring speeds, rolling element numbers, and lubricant materials. The study's findings offer a theoretical foundation for additional investigation into the contact between fluid and solid inside rolling bearings.

2. Theoretical formulation

2.1. Basic fluid equations

The fluid medium is set as an adiabatic incompressible viscous fluid without considering the temperature change. The equation of fluid continuity between the inner and outer rings of the bearing can be expressed as:

$$\frac{\partial}{\partial x_i}\left(\boldsymbol{u}_i\right) = 0, \tag{1}$$

where $\boldsymbol{u}_i$ is the velocity vector.

The momentum equation of the fluid can be expressed as:

$$\frac{\partial\left(\boldsymbol{u}_i\right)}{\partial t} + \frac{\partial\left(\boldsymbol{u}_i\boldsymbol{u}_j\right)}{\partial x_i} = -\frac{1}{\rho}\frac{\partial p}{\partial x_i} + \frac{\mu}{\rho}\frac{\partial}{\partial x_j}\left(\frac{\partial \boldsymbol{u}_i}{\partial x_i}\right) + S_i\,, \tag{2}$$

where μ is the micro-element fluid viscosity, p is the micro-element fluid pressure, andS_i is the generalized source term. Since the set of equations formed by the continuous and momentum equations is not a closed set of equations, supplementary equations are needed to solve the set of equations. The high speed of the bearing will make the fluid in the bearing cavity turbulent, which can easily produce a vortex under the action of fluid viscosity and wall surface. For the strong turbulence phenomenon between the inner and outer rings of the bearing, the RNG k-ε turbulence model is chosen for the entire fluid area control equation to close the set of equations. The model has a good simulation performance for the phenomena of rotational flow, boundary layer flow, and flow separation, and the k equation and ε equation of the model are expressed as [13]:

$$\frac{\partial}{\partial t}(\rho k) + \frac{\partial}{x_i}\left(\rho k \boldsymbol{u}_i\right) = \frac{\partial}{x_j}\left[\left(\mu + \frac{\mu_t}{\sigma_k}\right)\frac{\partial k}{\partial x_j}\right] + G_k - \rho\varepsilon - Y_m + G_b + S_k\,, \tag{3}$$

$$\frac{\partial}{\partial t}(\rho\varepsilon) + \frac{\partial}{x_i}\left(\rho\varepsilon \boldsymbol{u}_i\right) = \frac{\partial}{x_j}\left[\left(\mu + \frac{\mu_t}{\sigma_\varepsilon}\right)\frac{\partial \varepsilon}{\partial x_j}\right] + C_{1\varepsilon}\frac{\varepsilon}{k}\left(G_k + C_{3\varepsilon}G_b\right) - C_{2\varepsilon}\rho\frac{\varepsilon^2}{k} + S_\varepsilon\,, \tag{4}$$

where k is the turbulent kinetic energy, ε is the turbulent kinetic energy dissipation rate, ρ denotes the density, G_k denotes the turbulent kinetic energy generated by the mean velocity gradient, G_b is the turbulent kinetic energy generated by buoyancy, Y_m indicates the fluctuation caused by excessive diffusion in compressible turbulence, $C_{1\varepsilon}$, $C_{2\varepsilon}$ are the model constants, where $C_{1\varepsilon} = 1.42$ and $C_{2\varepsilon} = 1.68$; σ_k and σ_ε are the inverse of the turbulent Prandtl number of turbulent kinetic energy k and dissipation rate ε. S_k and S_ε denote custom parameters. In the above equations, i and j are taken as 1, 2, 3.

2.2. Fluid-structure interaction equation

The conservation equation for the solid part is derived from Newton's second law, which can be written as the following equation:

$$\rho_s \ddot{d}_s = \nabla * \sigma_s + f_s \,, \tag{5}$$

where ρ_s is the density of the solid; σ_s is the Cauchy stress tensor; f_s is the externally applied volume force vector; $\ddot{d}_s$ is the acceleration vector at the location of the solid.

Fluid-structure interaction follows the most fundamental conservation principle; at the intersection of fluid-solid coupling, should meet the fluid and solid stress τ, displacement d, and other variables of equal (subscript f indicates fluid, s indicates solid) that should meet the following equation:

$$\begin{aligned} \tau_f \, n_f &= \tau_s \, n_s \,, \\ d_f &= d_s \,, \end{aligned} \tag{6}$$

where d_f and d_s are the fluid and structural displacements, respectively, and are the fluid and structural stresses, respectively. The underlining of the symbols indicates that these values are defined only at the fluid-structure coupled interface.

A simultaneous solution method is used to couple the fluid and solid to solve for the variables. The sets of control equations for the fluid and solid domains are combined and linearized into one equation [14]:

$$\begin{bmatrix} \mathbf{A}_{ff} & \mathbf{A}_{fs} \\ \mathbf{A}_{sf} & \mathbf{A}_{ss} \end{bmatrix} \begin{bmatrix} \Delta \mathbf{X}_f^k \\ \Delta \mathbf{X}_s^k \end{bmatrix} = \begin{bmatrix} \mathbf{B}_f \\ \mathbf{B}_s \end{bmatrix}, \tag{7}$$

where $\mathbf{A}_{ff}$, $\Delta \mathbf{X}_f^k$, and $\mathbf{B}_f$ are the system matrix, the solution of the fluid domain, and the force, respectively. Similarly, $\mathbf{A}_{ss}$, $\Delta \mathbf{X}_s^k$ and $\mathbf{B}_s$ are the corresponding values in the solid domain, and $\mathbf{A}_{fs}$ and $\mathbf{A}_{sf}$ represent the coupling matrix. The displacement and stress criteria are chosen to control the convergence of the coupled system equations. If the differences in fluid velocity, pressure, temperature, and final rotor position are less than 0.001, the calculation is determined to be converged.

3. Computational models

3.1. Model building

The model 7005C angular contact bearing is selected as the object of study, and its structural parameters of the bearing are shown in Table 1. Considering the motion characteristics of rolling bearings, the periodic condition is used for the analysis; the inner ring only retains the inner wall; balls and cages are represented by their wall surfaces. The bearing model is shown in Fig. 1.

Table 1. Geometric parameters of 7005C

Parameter	Symbol	Value
Bearing outer diameter	D_o	47 mm
Bearing inner diameter	D_i	25 mm
Bearing width	B	12 mm
Ball diameter	D_b	6.35 mm
Number of balls	N	12
Angle of contact	α	15°

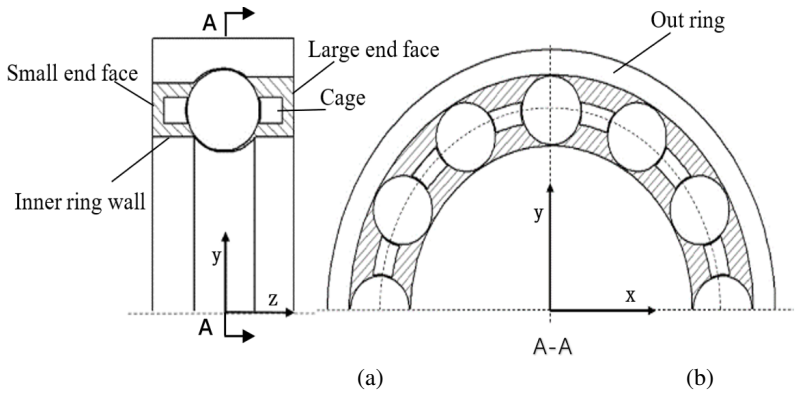

Fig. 1. Simplified diagrams of the model for different cross-sectional positions: (a) $X = 0$ cross-section, (b) $Z = 0$ cross-section

According to the geometry parameters of the bearing, the bearing finite element model is established. Fig. 2a is a fluid domain finite element model, which is coupled with the solid domain model. The mesh uses a tetrahedral grid, and the number of grids is about 3 million. As shown in Fig. 2b, the number of solid domain grids is about 700 000. The solid domain material is GCR15, and the material parameters are shown in Table 2. The minimum orthogonal quality of the grid is greater than 0.3, which meets the FLUENT computing requirements.

Table 2. GCr15 material properties

Parameter	Value
Density ρ (kg/m^3)	7830
Elastic modulus E (MPa)	208 000
Yield strength σ (MPa)	1370
Poisson ratio	0.3
Hardness (HB)	740

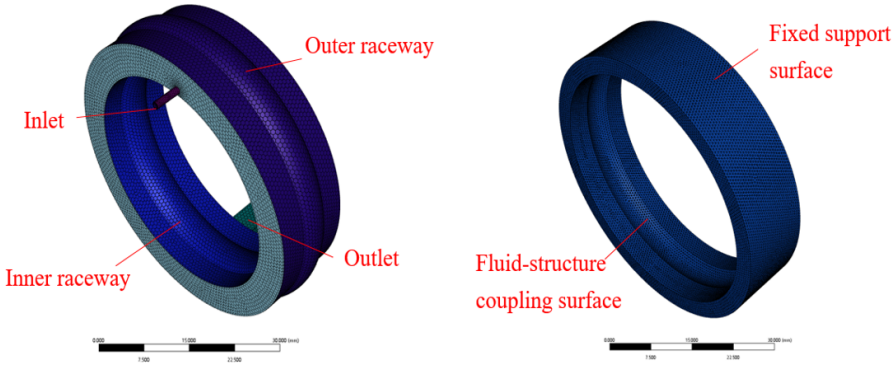

(a) fluid domain mesh (b) solid domain mesh

Fig. 2. Model mesh

3.2. Calculation settings

Considering the complexity of bearings during motion, the multi reference system model is selected. Different boundary conditions are used for different orientations of the bearings. The inlet boundary of the calculation domain is set as pressure inlet, taking the value of 4 MPa. The outlet boundary of the calculation domain is set as pressure outlet, taking the standard atmospheric pressure; the temperature is set as the default value; the inner ring and the wall of the rotating part are used as the rotation boundary; the standard rotational speed of the ball and cage is expressed as:

$$n_m = \frac{n_i}{2}\left(1 - \frac{D_w \cos\alpha}{d_m}\right), \tag{8}$$

where n_i is the inner ring speed; d_m is the pitch diameter of bearing; α is the contact angle; D_w is the diameter of the ball. The rotation speed of the ball is achieved by setting different velocity boundaries on their outer surface. The standard wall function is applied to the area near the wall, while the other wall surfaces are considered adiabatic, solid, and non-sliding boundaries. ANSYS FLUENT and ANSYS Transient Structural are used as the tools to solve CFD and structural

problems, respectively, using a bidirectional FSI approach. Unlike unidirectional FSI, bidirectional FSI updates the flow conditions according to the structural deformation during the CFD and finite element analysis iterations. The flow diagram of the bidirectional FSI solution used here is shown in Fig. 3.

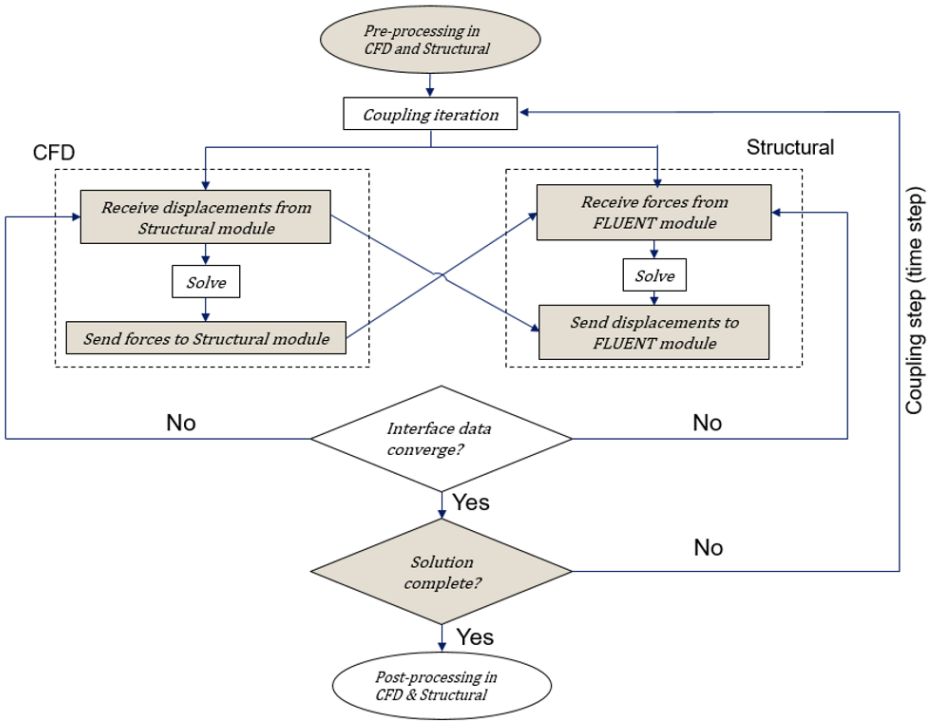

Fig. 3. Bidirectional FSI procedure

4. Calculation results and analysis

4.1. Pressure distribution

According to the operating conditions of 7005C, the bearing inner ring speed of 1.5×10^4 rpm, and the lubricant of No. 4106 aviation lubricant with a density of 876 g/cm^3 and a viscosity of 18.24 mm^2/s are selected as the standard working condition.

Fig. 4 shows the pressure cloud diagram of the axial coordinate $Z = 0$ section under standard working conditions. Because the inner ring of the bearing rotates counterclockwise and the ball of the bearing rotates clockwise, vortex flow will be generated near the gap between the ball and the inner ring. It causes that the lubricant cannot enter the gap smoothly, thus creating negative pressure at the gap location. Because the outer ring remains fixed, there is a positive pressure area on

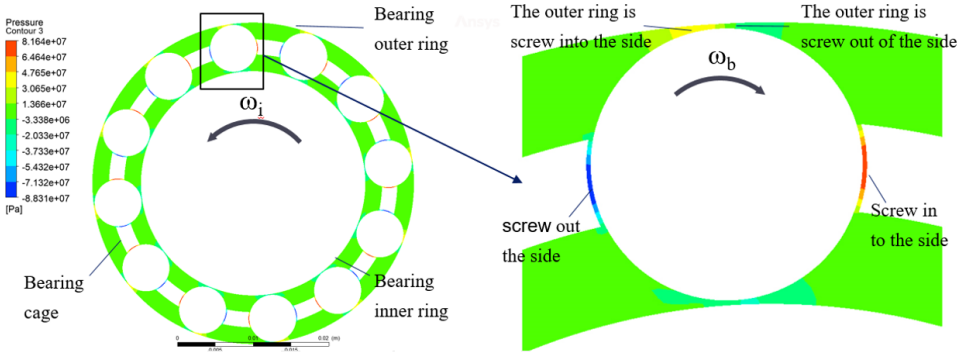

Fig. 4. Pressure cloud diagram of the $Z = 0$ section of the bearing flow field

the screw-in side and a negative pressure area on the screw-out side. The rotation of the ball drives the fluid to move in the screw-in side area, which makes the gap between the ball and the cage generating a larger positive pressure. By the same token, it can be seen that the lubricant enters more into the screw-in side area, thus generating a larger negative pressure on the screw-out side of the gap between the ball and the cage. Because the lubricant at the gap between the cage and the ball is obviously more squeezed, the pressure is greatest here.

Fig. 5 shows the pressure cloud diagram of the axial coordinate $X = 0$ section under standard working conditions. The cross-sectional pressure change away from the ball is relatively gentle, and the cross-sectional change near the ball has a large amplitude. Because there is a negative pressure area in the contact area between the bearing inner ring and the balls, placing the oil inlet close to the bearing inner ring facilitates the smooth entry of the lubricating oil into the bearing chamber.

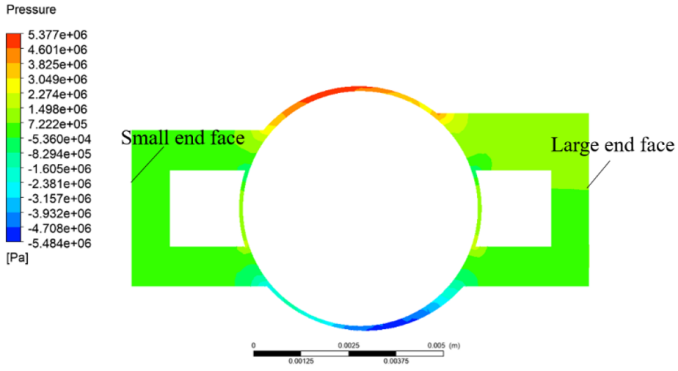

Fig. 5. Pressure cloud diagram of the $X = 0$ section of the bearing flow field

Fig. 6 shows the average pressure-time diagram of the two end surfaces of the bearing size under transient calculation. As the running time of the bearing increases, the average pressure at the large end of the bearing gradually exceeds

that at the small end, and the difference between them gradually increases. This is because the cage is close to the small end, which makes the linear velocities at the two ends different, and also makes the pressure between the large and small ends of the bearing different. Therefore, small-end oiling is more suitable for high-speed bearings, which is consistent with the conclusion of the analysis by Liu [15].

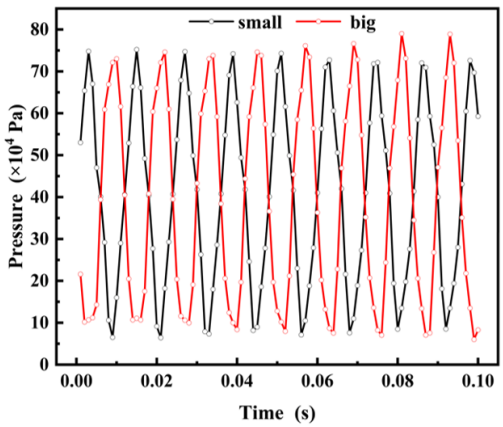

Fig. 6. Average pressure-time diagrams of bearing large and small end faces

4.2. Velocity distribution

Due to its multiple balls and turbulent flow conditions, the flow field distribution inside the bearing chamber is an important factor affecting the lubrication performance of angular contact ball bearings. Under standard operating conditions, the velocity-flow distribution is shown in Fig. 7. With time, the fluid motion gradually smooths out and the velocity reaches its maximum at the ball surface.

Fig. 8 shows the vector distribution of the bearing flow field after it have reached a steady state. The vortex occurs in the bearing flow field in the load-bearing zone. The vortex causes fluid discontinuity in the load-bearing zone, which reduces the bearing capacity.

Fig. 9 shows the effect between velocity and coordinates at a speed of 1.5×10^4 rpm, depending on the distance between the coordinate point and the ball, $Z = 2$~6. In the dimensionless coordinates of Fig. 9a, the velocity variation at $Z = 6$ is relatively flat, which is favorable for oil injection into the bearing chamber. The results of comparing the velocity variation of the cross section at different radial positions along the Y axis in Fig. 9b show that the velocity variation is higher near the inner ring at 1 mm, which is favorable for the oil to enter the bearing chamber [15].

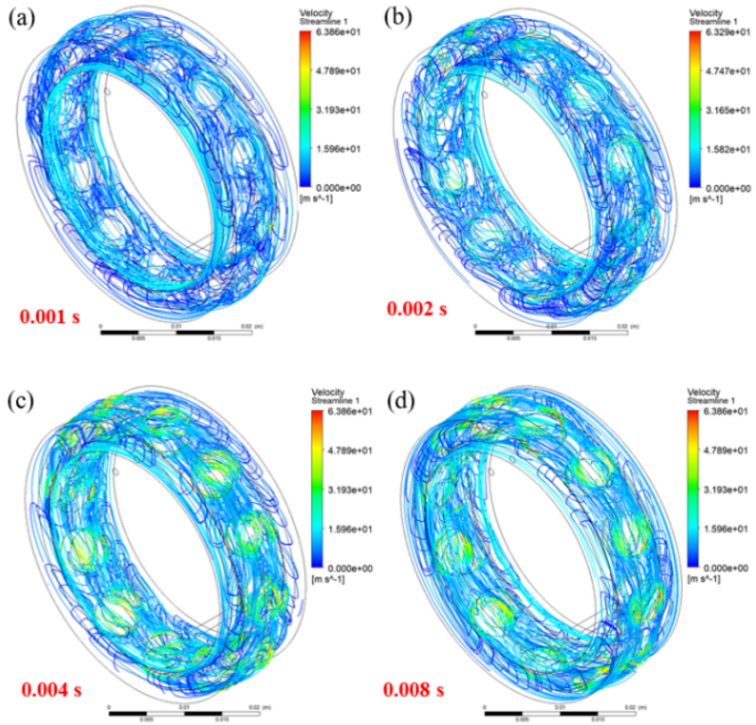

Fig. 7. Cloud map of flow velocity distribution in a transient state: (a) t = 0.001 s, (b) t = 0.002 s, (c) t = 0.004 s, (d) t = 0.008 s

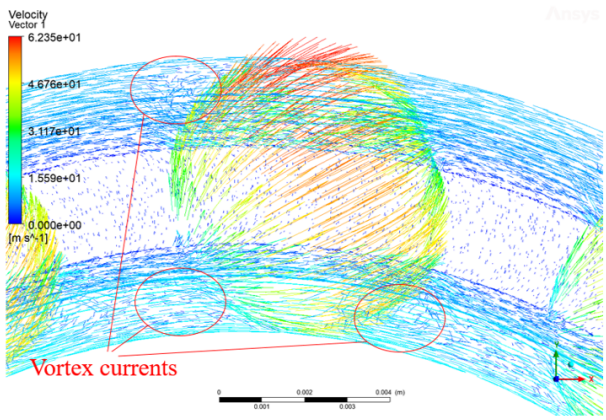

Fig. 8. Flow field vector distribution picture

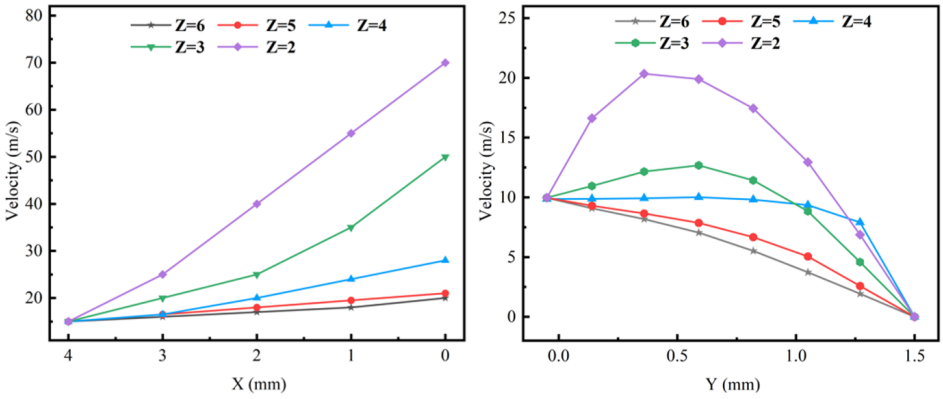

(a) different X coordinates (b) different Y coordinates

Fig. 9. The plot of velocity coordinates for different axial positions at 1.5×10^4 rpm

4.3. Rotational speed variation effect

Taking 5×10^3, 1.0×10^4, 1.5×10^4, and 2.0×10^4 rpm as the calculation example, Fig. 10 shows the lubricating oil film pressure of the balls subjected to the maximum load of angular contact ball bearings in contact with the outer ring. The pressure fluctuation area and amplitude increase with the increase of rotational speed. The lubricating oil film velocity distribution is shown in Fig. 11, with the increase of rotational speed, the speed fluctuation area and the peak increase.

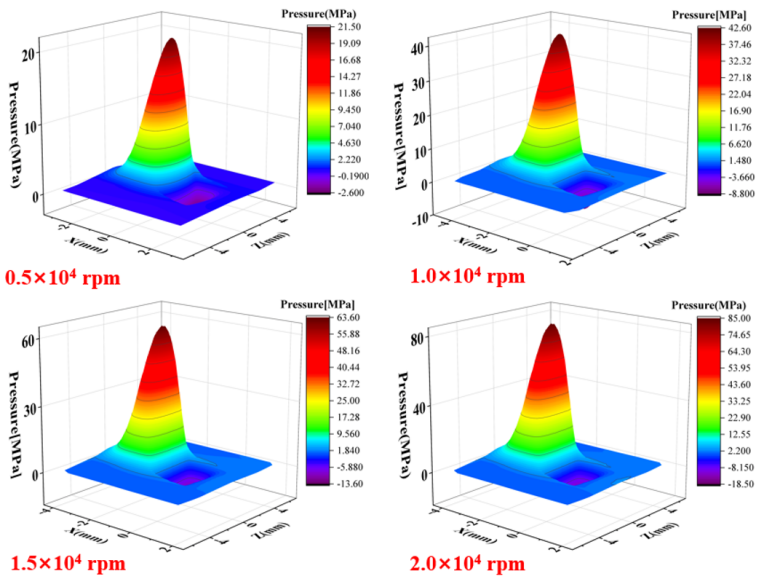

Fig. 10. Three-dimensional distribution of lubricant film pressure at different speeds

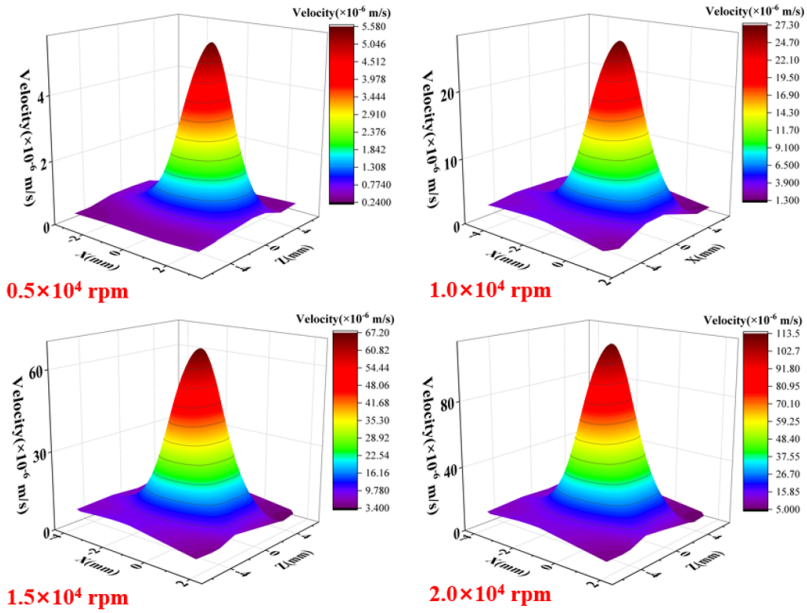

Fig. 11. Three-dimensional distribution of lubricant film velocity at different speeds

Fig. 12 shows the velocity and pressure distribution of the lubricating oil film along the *X*-axis at different speeds. As shown in Fig. 12a, the surface pressure of the lubricating oil first increases and then decreases along the *X*-axis, which is consistent with the above pressure analysis. As shown in Fig. 12b, at different speeds, the velocity distribution on the surface of the lubricating oil film remains unchanged, and it is still the fastest in the area with the thinnest oil film. With the increase in speed, the ball drives the lubricating oil to the outer ring to spiral into

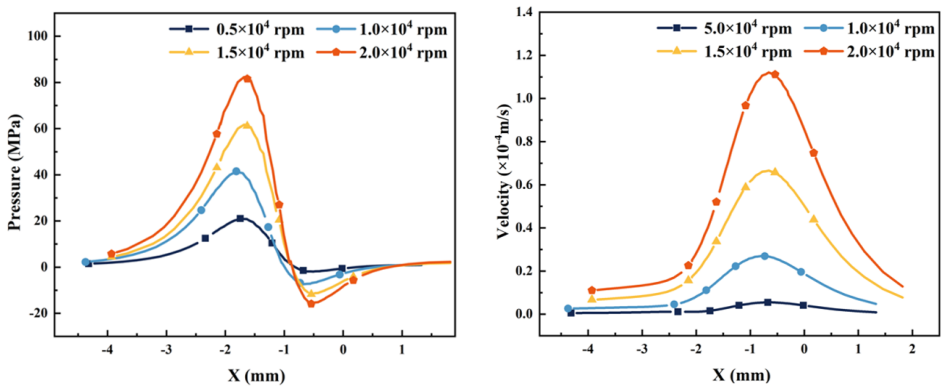

(a) pressure (b) velocity

Fig. 12. Pressure and velocity distribution of lubricating oil film along the *X*-axis at different speeds

the side more quickly, resulting in an increase in the surface pressure of the oil film of the outer ring. At the same time, as the lubricant accumulates on the screw-in side, it is unable to pass through the gap between the balls and the outer ring in time, which leads to an increase in the negative pressure value on the screw-out side of the outer ring.

With 5×10^3, 1.0×10^4, 1.5×10^4, and 2.0×10^4 rpm as an example, based on the fluid-solid coupling analysis method, the angular contact ball bearings with maximum load ball and outer ring contact bearing outer ring stress distribution are as shown in Fig. 13. With the increase of speed, the stress on the outer ring surface of the bearing increases, and the stress distribution remains unchanged.

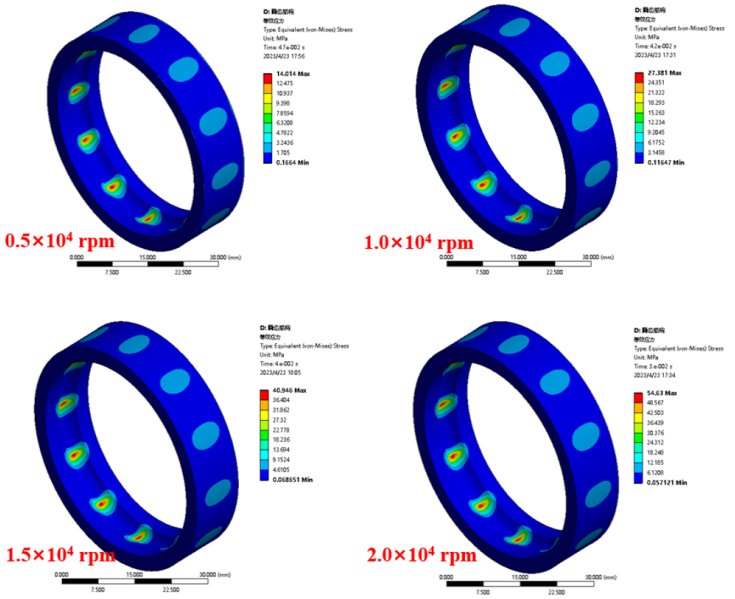

Fig. 13. Bearing outer ring pressure clouds at different speeds

At the location of the maximum contact load between the ball and the outer ring in the bearing, the distribution of equivalent stresses in the outer ring along the X-axis is shown in Fig. 14. During the operation of the bearing, a large amount of lubricant is rolled into the contact position between the ball and the outer ring of the bearing. Due to the fact that contact position clearance is small, the velocity vector of lubricant into the bearing clearance changes greatly, and the corresponding force needs to be given to the outer ring of the bearing to change the velocity vector, so the outer ring stress in the contact position (the thinnest area of the oil film) is the largest.

In Fig. 15, there are shown, at different speeds, the balls surface velocity distribution of the angular contact ball bearing with the maximum load when the balls are in contact with the outer ring. The pressure distribution is shown in Fig. 16.

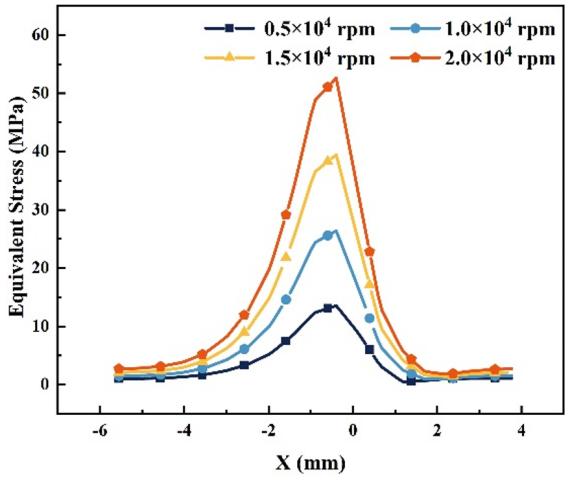

Fig. 14. Equivalent stress distribution of bearing outer ring along X-axis at different speeds

The balls surface velocity is a spherical distribution, and the pressure on the balls surface is the positive pressure area on the screw-in side and the negative pressure on the screw-out side.

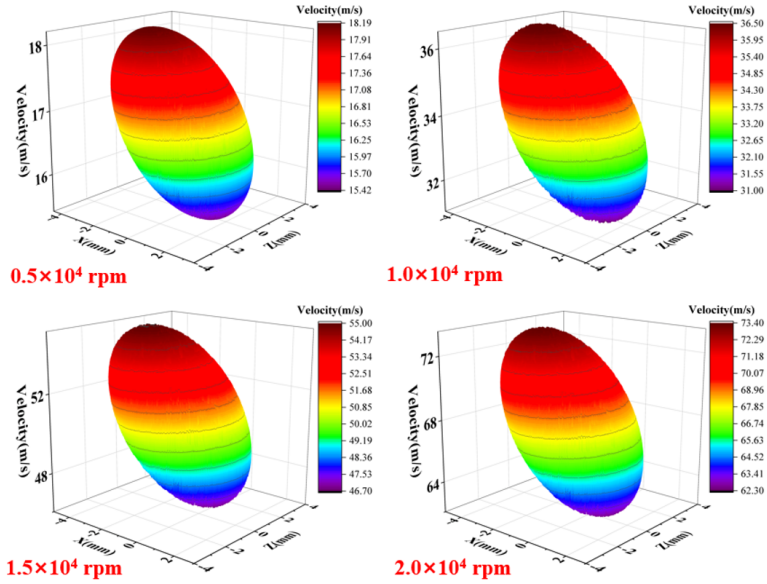

Fig. 15. Three-dimensional distribution of oil film velocity on the ball surfaces at different speeds

Fig. 17 shows the pressure and velocity distribution of the ball surface at different speeds. As the bearing speed increases, the variation pattern of oil film pressure and velocity distribution is consistent. As the speed increases, the speed

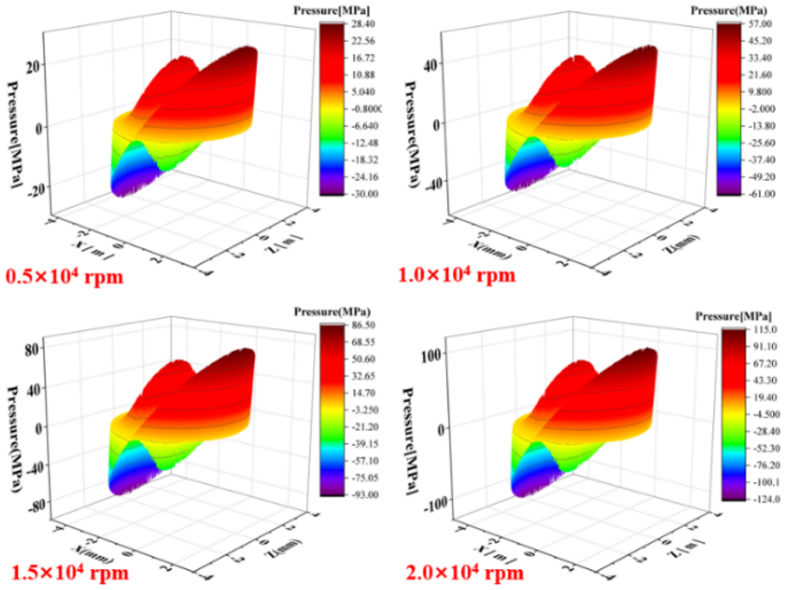

Fig. 16. Three-dimensional distribution of oil film pressure on the ball surfaces at different speeds

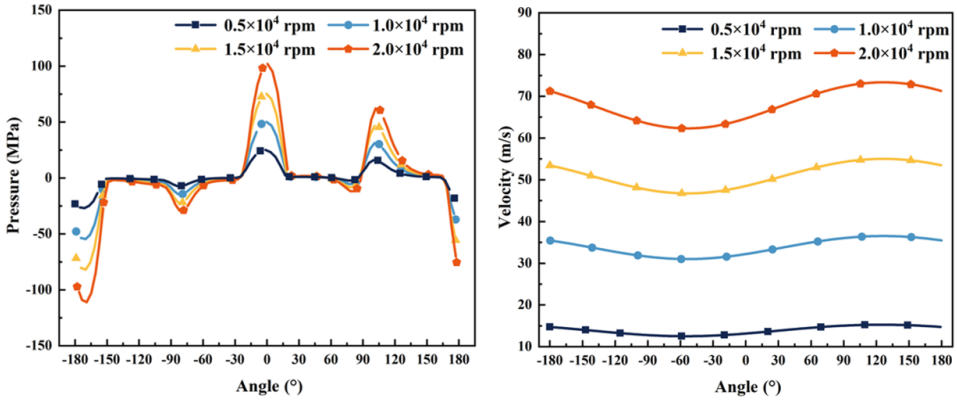

Fig. 17. The pressure and velocity distribution of the ball surface of the bearing at different speeds

of the lubricant film on the surface of the ball increases, and the ball brings more lubricant into the gap at the same time, so that the value of the pressure on the screw-in side and the value of the negative pressure on the screw-out side both increase.

4.4. Lubricant parameters variation effect

The parameters of the lubricants are changed under standard operating conditions. Six lubricants with high kinematic viscosity were selected for the calculation, and the material parameters are shown in Table 3.

Table 3. Lubricating oil parameters

Lube oil number	Density ρ [kg/m^3]	Viscosity [mm^2/s]
No. 1	876	30
No. 2	897	22
No. 3	925	19.7
No. 4	950	18.4
No. 5	970	15.6
No. 6	997	12.4

The distribution of the lubricant film pressure and velocity along the X-axis of the angular contact ball bearing maximum load ball in contact with the outer ring is shown in Fig. 18. As the viscosity of the lubricant decreases, the lubricant passes more easily through the oil film gap, and the speed and pressure of the lubricant on the surface of the outer ring decreases gradually.

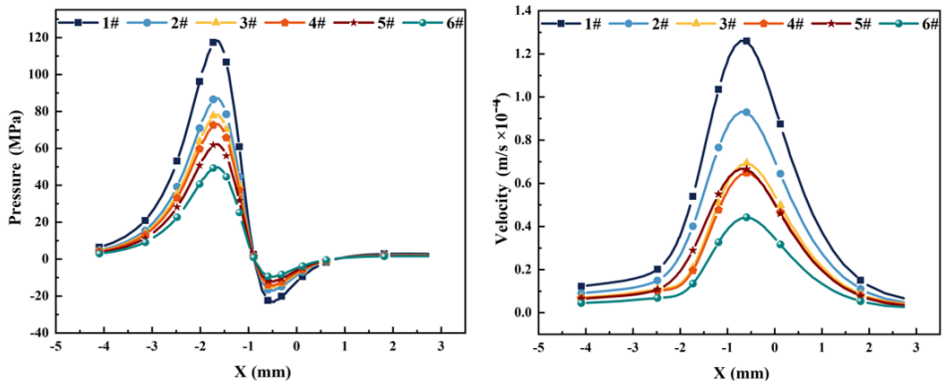

Fig. 18. Pressure and velocity distribution of lubricating oil on the bearing outer ring surface along the X-axis for different lubricant parameters

The distribution of equivalent stresses on the outer ring of the bearing at the maximum loaded ball position along the X-axis is shown in Fig. 19. As the viscosity of the lubricant decreases, the change in velocity vector as the lubricant enters the bearing gap decreases, the force required to be supplied by the outer ring decreases, and therefore the equivalent stress on the outer ring decreases.

Fig. 20 shows the pressure and velocity distribution of the ball surface at different lubricant parameters. As shown in Fig. 20, similar to the outer ring surface pressure variation, the decrease in lubricant viscosity caused the ball surface pressure to decrease. However, the lubricant parameters have a lesser effect on the ball surface velocity.

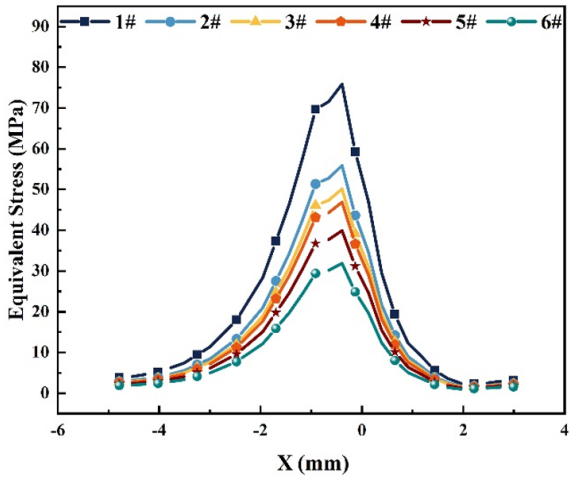

Fig. 19. Equivalent stress distribution of bearing outer ring along X-axis at different lubricant parameters

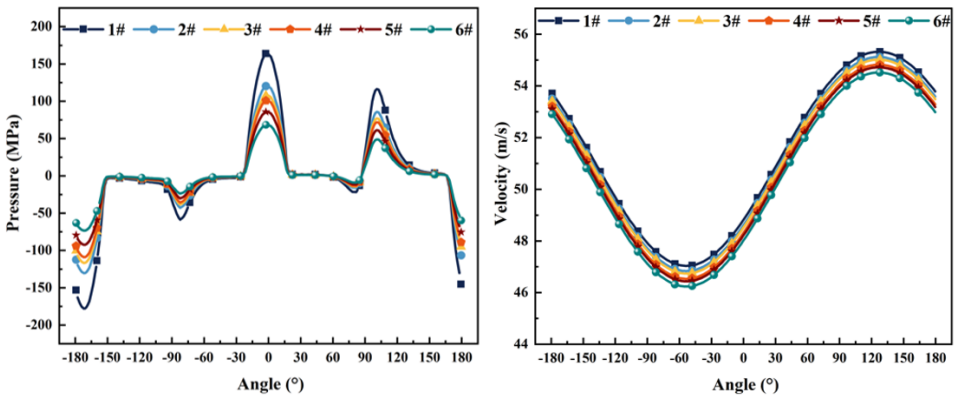

Fig. 20. The pressure and velocity distribution of the bearing ball surface at different lubricant parameters

4.5. Balls number variation effect

Different numbers of balls were selected under standard operating conditions of the bearings, and their effects on the lubrication and contact characteristics of the bearings were investigated. The distribution of lubricant pressure and velocity on the outer ring surface of the bearing at different numbers of balls are shown in Fig. 21. According to the data in the figure, the change in the ball numbers only affects the distribution position of the oil film pressure and velocity on the outer ring surface, and it has a small effect on its value.

For the calculation of the solid domain aspect, Fig. 22 shows the stress distribution of the outer ring at different ball numbers, and Fig. 23 shows the equivalent

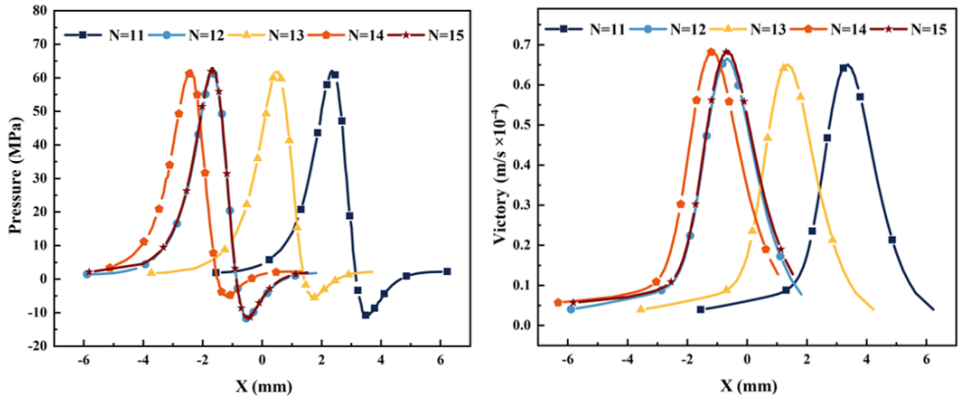

Fig. 21. Pressure and velocity distribution of lubricating oil on the bearing outer ring surface along the X-axis at different ball numbers

stress variation along the X-axis in the stress concentration region of the outer ring. Combining the results of Fig. 23 and Fig. 24, it can be seen that the increase in the number of balls makes that the area of stress concentration on the surface of the raceway increases, while the maximum stress value is only slightly reduced. It indicates that the effect of the ball numbers on the lubricant pressure is minimal, while the main factors affecting the lubricant pressure are the fluid velocity and the lubricant properties.

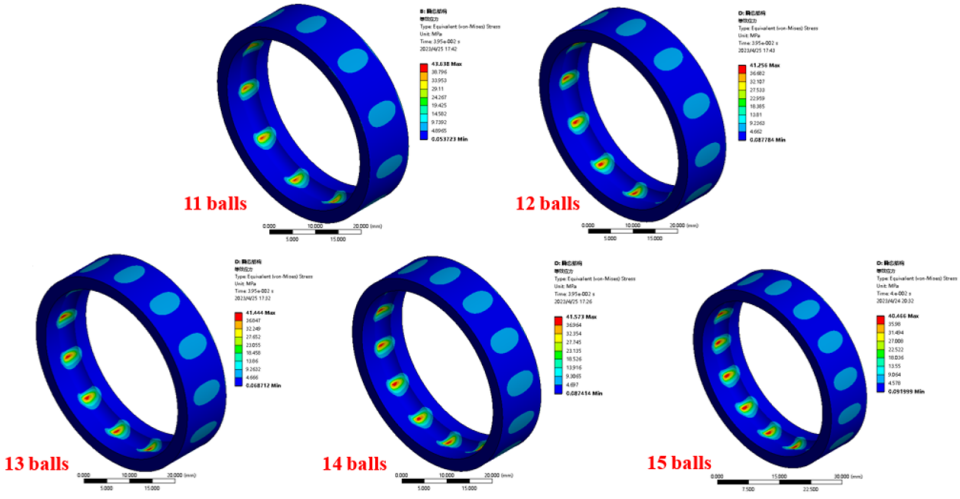

Fig. 22. Stress distribution of the outer ring under different number of balls

Fig. 24 shows the pressure and velocity distribution of the lubricant on the ball surface at different ball numbers. It can be seen from the figure that the pressure and velocity distribution of the lubricant on the balls surface produces the same trend, while the pressure values and velocity values do not change significantly.

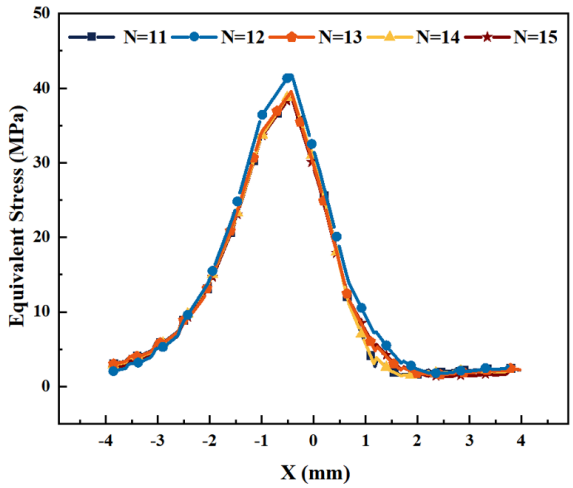

Fig. 23. Equivalent stress distribution of bearing outer ring along X-axis at different numbers of balls

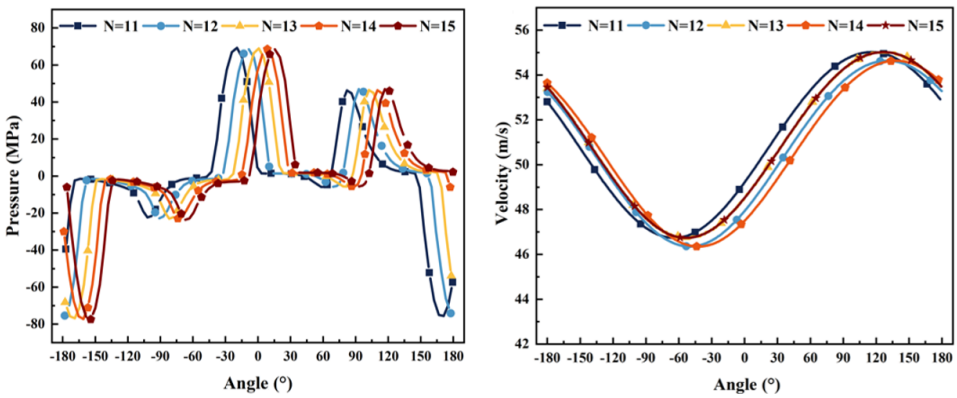

Fig. 24. The pressure and velocity distribution of the ball surface of the bearing at different number of balls

5. Conclusions

In order to analyze the lubrication characteristics of angular contact ball bearings, a fluid-solid coupling analysis model was established to calculate the influence of working condition parameters on the internal contact characteristics, and the main conclusions are as follows:

1. The lubricant at the gap between the cage and the ball is squeezed, and the oil film pressure in the bearing cavity is maximum
2. Oiling at the small end of the bearing near the inner ring can reduce the influence of turbulence on the lubricant at high speed and help the lubricant

enter the bearing cavity. The best location for oiling is the small end face just about 1 mm from the inner ring of the bearing.

3. Adding the lubricant from the small end face of the bearing near the inner ring reduces the effect of turbulence on the lubricant at high speeds, which helps the lubricant to enter the bearing cavity. The best place to add lubricant is the small end face of the bearing approximately 1 mm from the inner ring.
4. Speed and lubricant parameters are the main factors affecting the pressure and speed of the lubricant film in the contact area inside the bearing. The lubricant film pressure will rise with increasing speed and viscosity of the lubricant.
5. The number of balls affects the pressure and velocity distribution of the flow field inside the bearing, but has a small effect on the values of the characteristic parameters of the bearing flow field.

Acknowledgements

The authors gratefully acknowledge the support from the Major scientific and technological projects in Shanxi Province (20201102003), Shanxi coal based low carbon joint fund (No. U1610118), National Natural Science Foundation of China (No. 51375325).

References

[1] B. Yan, L. Dong, K. Yan, F. Chen, Y. Zhu, and D. Wang. Effects of oil-air lubrication methods on the internal fluid flow and heat dissipation of high-speed ball bearings. *Mechanical Systems and Signal Processing*, 151:107409, 2021. doi: 10.1016/j.ymssp.2020.107409.

[2] H. Bao, X. Hou, X. Tang, and F. Lu. Analysis of temperature field and convection heat transfer of oil-air two-phase flow for ball bearing with under-race lubrication. *Industrial Lubrication and Tribology*, 73(5):817–821, 2021. doi: 10.1108/ilt-03-2021-0067/v2/decision1.

[3] T.A. Harris. *Rolling Bearing Analysis*. Taylor & Francis Inc. 1986.

[4] T.A. Harris and M.N. Kotzalas. *Advanced Concepts of Bearing Technology*. Taylor & Francis Inc. 2006.

[5] F.J. Ebert. Fundamentals of design and technology of rolling element bearings. *Chinese Journal of Aeronautics*, 23(1):123-136, 2010. doi: 10.1016/s1000-9361(09)60196-5.

[6] T.A. Harris. An analytical method to predict skidding in high speed roller bearings. *A S L E Transactions*, 9(3):229–241, 1966. doi: 10.1080/05698196608972139.

[7] A. Wang, S. An, and T. Nie. Analysis of main bearings lubrication characteristics for diesel engine. In: *IOP Conference Series: Materials Science and Engineering*, 493(1):012135, 2019. doi: 10.1088/1757-899X/493/1/012135.

[8] W. Zhou, Y. Wang, G. Wu, B. Gao, and W. Zhang. Research on the lubricated characteristics of journal bearing based on finite element method and mixed method. *Ain Shams Engineering Journal*, 13(4):101638, 2022. doi: 10.1016/j.asej.2021.11.007.

[9] J. Chmelař, K. Petr, P. Mikeš, and V. Dynybyl. Cylindrical roller bearing lubrication regimes analysis at low speed and pure radial load. *Acta Polytechnica*, 59(3):272–282, 2019. doi: 10.14311/AP.2019.59.0272.

[10] C. Wang, M. Wang, and L. Zhu. Analysis of grooves used for bearing lubrication efficiency enhancement under multiple parameter coupling.*Lubricants*, 10(3):39, 2022. doi: 10.3390/lubricants10030039.

[11] Z. Xie and W. Zhu. An investigation on the lubrication characteristics of floating ring bearing with consideration of multi-coupling factors. *Mechanical Systems and Signal Processing*, 162:108086, 2022. doi: 10.1016/j.ymssp.2021.108086.

[12] M. Almeida, F. Bastos, and S. Vecchio. Fluid–structure interaction analysis in ball bearings subjected to hydrodynamic and mixed lubrication. *Applied Sciences*, 13(9):5660, 2023. doi: 10.3390/app13095660.

[13] J. Sun, J. Yang, J. Yao, J. Tian, Z. Xia, H. Yan, and Z. Bao. The effect of lubricant viscosity on the performance of full ceramic ball bearings. *Materials Research Express*, 9(1):015201, 2022. doi: 10.1088/2053-1591/ac4881.

[14] D.Y. Dhande and D.W. Pande. A two-way FSI analysis of multiphase flow in hydrodynamic journal bearing with cavitation. *Journal of the Brazilian Society of Mechanical Sciences and Engineering*, 39:3399–3412, 2017. doi: 10.1007/s40430-017-0750-8.

[15] H. Liu, Y. Li, and G. Liu. Numerical investigation of oil spray lubrication for transonic bearings. *Journal of the Brazilian Society of Mechanical Sciences and Engineering*, 40:401, 2018. doi: 10.1007/s40430-018-1317-z.